Magnetic, orbital, and charge ordering in the electron-doped manganites

Tulika Maitra[1,*] and A. Taraphder[2,†]
[1]*Max-Planck-Institut für Physik Komplexer Systeme, Nöthnitzer Str. 38, 01187 Dresden, Germany*
[2]*Department of Physics and Meteorology and Centre for Theoretical Studies, Indian Institute of Technology, Kharagpur 721302, India*

(Received 3 January 2003; revised manuscript received 26 June 2003; published 11 November 2003)

The three-dimensional perovskite manganites $R_{1-x}A_xMnO_3$ in the range of hole doping $x>0.5$ are studied in detail using a double-exchange model with degenerate e_g orbitals including intraorbital and interorbital correlations and near-neighbor Coulomb repulsion. We show that such a model captures the observed phase diagram and orbital ordering in the intermediate- to large-bandwidth regimes. It is argued that the Jahn-Teller effect, considered to be crucial for the region $x<0.5$, does not play a major role in this region, particularly for systems with moderate to large bandwidths. The anisotropic hopping across the degenerate e_g orbitals is essential for the understanding of the ground-state phases of this region, an observation emphasized earlier by Brink and Khomskii. Based on calculations using a realistic limit of finite Hund's coupling, we show that the inclusion of interactions stabilizes the *C* phase, and the antiferromagnetic metallic *A*-phase moves closer to $x=0.5$ while the ferromagnetic phase shrinks, in agreement with recent observations. The charge ordering close to $x=0.5$ and the effect of reduction of bandwidth are also outlined. The effect of disorder and the possibility of inhomogeneous mixture of competing states are discussed.

DOI: 10.1103/PhysRevB.68.174416 PACS number(s): 75.30.Et, 75.47.Lx, 75.47.Gk

I. INTRODUCTION

The colossal magnetoresistive manganites have been investigated with renewed vigor in the recent past mainly because of their technological importance. It was soon realized that these systems have a rich variety of unusual electronic and magnetic properties involving almost all the known degrees of freedom in a solid, viz., the charge, spin, orbital, and lattice degrees of freedom.[1–3] Of particular interest have been the systems $R_{1-x}A_xMnO_3$, where *R* and *A* stand for trivalent rare-earth (e.g., La, Nd, Pr, Sm) and divalent alkaline-earth (Ca, Sr, Ba, Pb, etc.) ions, respectively. Around the region $0.17<x<0.4$, electrical transport properties of these systems generically show extreme sensitivity towards external magnetic fields with a concomitant paramagnetic insulator (or poor metal) to ferromagnetic metal transition at fairly high temperatures (see Ref. 3 and references therein). For a long time the dominant paradigm in the theory of this unusual magnetic field dependence of transport has been the idea of *double exchange*[4] (DE) involving the localized core spins coupled to the itinerant electrons in the Jahn-Teller split e_g level via strong Hund's exchange. It has been realized recently that such a simplifying theoretical framework may not be adequate to explain several other related features involving transport, electronic, and magnetic properties.[5–9] It was already known that the observed structural distortions and magnetic and orbital orders in these systems in the region $x\simeq 0.5$ require interactions not included in the DE model.[10,11]

Owing to the observation of colossal magnetoresistance (CMR) in the region $x<0.5$ in the relatively narrow-band width materials at high temperatures, much of the attention was centered around this region. Only in the last few years has the CMR effect been observed in the larger-bandwidth materials like $Nd_{1-x}Sr_xMnO_3$ (Refs. 12 and 13) and $Pr_{1-x}Sr_xMnO_3$ (Refs. 14 and 15) in the region $x>0.5$. If one counts the doping from the side $x=1$ in $R_{1-x}A_xMnO_3$ where all Mn ions are in $+4$ state, then doping by R_y $(y=1-x)$ introduces Mn^{3+} ions carrying one electron in the e_g orbitals. This region, therefore, is also called the *electron-doped region*. The charge, magnetic, and orbital structures of the manganites in the electron-doped regime have already been found to be quite rich[16–18] and the coupling between all these degrees lead to stimulating physics.[19]

In the framework of the conventional DE model with one e_g orbital, one would expect qualitatively similar physics for $x\sim 0$ and $x\sim 1$. On the contrary, experiments reveal a very different and asymmetric picture for the phase diagram between the regions $x<0.5$ and $x>0.5$. The lack of symmetry about $x=0.5$ manifests itself most clearly in the magnetic phase diagram of these manganites. It has now been shown quite distinctly[13,20–22] that the systems $Nd_{1-x}Sr_xMnO_3$, $Pr_{1-x}Sr_xMnO_3$, and $La_{1-x}Sr_xMnO_3$ are antiferromagnetically ordered beyond $x=0.5$ while one observes either a metallic ferromagnetic state or a charge ordered state with staggered charge ordering[23] in the approximate range $0.25<x<0.5$. This charge-ordered insulating state can be transformed into a ferromagnetic metallic state[2,14] by the application of magnetic fields.

There are several different types of antiferromagnetic (AFM) phases with their characteristic dimensionality of spin ordering observed in this regime. $La_{1-x}Sr_xMnO_3$ shows an *A*-type antiferromagnetic ground state (in which ferromagnetically aligned *xy* planes are coupled antiferromagnetically) in the range $0.52<x<0.58$. It also shows a sliver of FM phase[20] immediately above $x=0.5$. In $Nd_{1-x}Sr_xMnO_3$ (Refs. 13 and 22), the *A*-type spin structure appears at $x=0.5$ and is stable up to $x=0.62$ while in $Pr_{1-x}Sr_xMnO_3$ (Refs. 14 and 24), this region extends from $x=0.48$ to $x=0.6$. In all these cases, the phase that abuts the *A*-type AFM in the region of higher hole doping is the *C*-type AFM state, in which antiferromagnetically

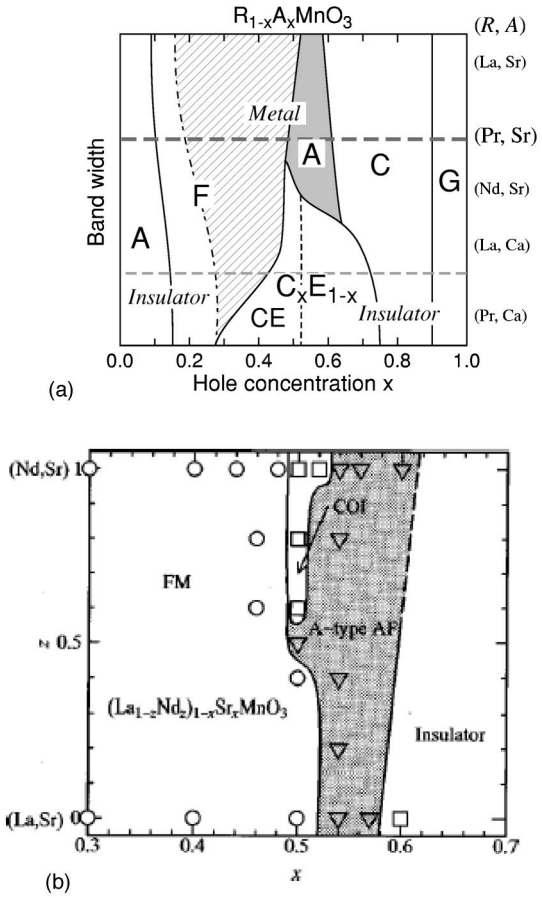

FIG. 1. (a) Schematic phase diagram in the bandwidth vs hole concentration plane in the series of three-dimensional manganites after Kajimoto *et al.* (Ref. 25). The labels represent different magnetic phases explained in the text. C_xE_{1-x} stands for an incommensurate charge-ordered and CE-type spin-ordered phase. In (b) is shown the phase diagram in z vs hole concentration plane for $(La_{1-z}Nd_z)_{1-x}Sr_xMnO_3$ after Akimoto *et al.* (Ref. 20). The effective bandwidth decreases as z increases. COI stands for charge-ordered insulating phase.

aligned planes are coupled ferromagnetically. The *C*-type AFM phase occupies the largest part of the phase diagram in this region. For even larger x, the *C* phase gives way to the three-dimensional antiferromagnetic *G* phase.

The systematics of the phase diagram changes considerably as a function of bandwidth in these systems. Recently Kajimoto *et al.*[25] have quite succinctly summarized the phase diagrams of various manganites of varying bandwidths across the entire range of doping. Such a phase diagram is shown schematically in Fig. 1(a) after Kajimoto *et al.*[25] The phase diagram changes considerably with changing bandwidth. We note that the narrow-bandwidth compounds like $Pr_{1-x}Ca_xMnO_3$, $La_{1-x}Ca_xMnO_3$, etc., exhibit a region of CE-type insulating charge-ordered (CO) state around $x=0.5$ whereas the intermediate-bandwidth material $Nd_{1-x}Sr_xMnO_3$ shows an *A*-type antiferromagnetic phase. As one moves towards the larger-bandwidth compounds such as $Pr_{1-x}Sr_xMnO_3$ and $La_{1-x}Sr_xMnO_3$, a small strip of ferromagnetic (*F*) metallic phase appears at $x=0.5$ (Refs. 20 and 25) followed by the *A*-type AFM state. In contrast with the narrow-bandwidth manganites, the relatively wider-bandwidth manganites generally show the following sequence of spin/charge ordering upon hole doping (in the entire range $0 \leqslant x \leqslant 1$): insulating *A*-type AFM $\rightarrow$ metallic FM$\rightarrow$metallic *A*-type AFM$\rightarrow$ insulating *C*-type AFM and finally insulating *G*-type AFM states. Clearly, the most important feature here is the absence of CE-type spin/charge ordering and the presence of a metallic *A*-type AFM state in these wider-bandwidth compounds in the region close to $x=0.5$. It appears that the physics involved in the CE-type charge/spin ordering, important for the low-bandwidth systems, is not quite as relevant in this case. In addition, it is also observed in neutron diffraction studies that the metallic *A*-type AFM state is orbitally ordered[21,22] with predominant occupation of $d_{x^2-y^2}$ orbitals. The importance of orbital ordering has been emphasized previously in several other experimental[13,26–28] and theoretical[29–33] investigations.

In a detailed observation carried out by Akimoto *et al.*[20] the electronic and magnetic properties of a heavily doped manganite $R_{1-x}Sr_xMnO_3$ with $R=La_{1-z}Nd_z$ are studied by continuously changing the bandwidth. They were able to control the bandwidth *chemically* by the substitution of the smaller Nd^{3+} ions for the larger La^{3+} ions. By increasing z, they were able to go continuously from the large-bandwidth $La_{1-x}Sr_xMnO_3$ down to the intermediate-bandwidth $Nd_{1-x}Sr_xMnO_3$ system. For $z<0.5$, there is a metallic FM phase in the region $0.5<x<0.52$. From $x \geqslant 0.54$ to about $x=0.58$ the ground state is *A*-type antiferromagnetic metallic irrespective of the value of z. They believe that the key factor that stabilizes the *A*-type AFM metallic state in such a wide range of z is the structure of the two e_g orbitals ($d_{x^2-y^2}$ and $d_{3z^2-r^2}$) and the anisotropic hopping integral between them. There is no signature of charge ordering or CE-type ordering below $z=0.5$ for any x. The CO insulating state appears above $z=0.5$ and around $x=0.5$ primarily due to the commensuration (between the lattice periodicity and hole concentration) effect in the low-bandwidth systems. The ground-state phase diagram for doped manganites in the x-z plane (i.e., *doping versus bandwidth* plane) is shown in Fig. 1(b) after Akimoto *et al.*[20]

The general inferences from all these measurements are that the physics of the electron-doped region is very different from the hole-doped region. In this region, with decreasing bandwidth starting from $La_{1-x}Sr_xMnO_3$ down to $Nd_{1-x}Sr_xMnO_3$, the *F* phase shrinks, and the *A* and *C* phases remain nearly unaffected. The *A* phase disappears and the *C* phase reduces rapidly in the low-bandwidth systems like $La_{1-x}Ca_xMnO_3$ and $Pr_{1-x}Ca_xMnO_3$. The *G* phase at the low-electron-doping region seems to remain unaffected all through. It has been seen[13,20,22,26] that the gradual buildup of AFM correlations in the electron-doped region is preempted by the orbital ordering in the *A* and *C* phases. The e_g orbitals and the anisotropic hopping of electrons between them,[11,34] must indeed play a significant role given the presence of orbital ordering in much of the phase diagram beyond $x=0.5$. It is also realized that the effect of lattice could be ignored in the first approximation for these moderate- to large-bandwidth systems in this region of doping.

There have been a large number of reports of charge or-

dering and inhomogeneous states[12,14,35–39] in the region $x \simeq 0.5$. These states are quite abundant in the low-bandwidth materials. The inhomogeneous states result from the competing ground states[5,40] (charge ordered/AFM and FM primarily) that lead to first-order phase transitions with a discontinuity in the density as the chemical potential is varied. Such transitions are known to lead to phase separation in the canonical ensemble.[41–46] Such macroscopic phase separations are not stable against long-range Coulomb interactions and tend to break up into microscopic inhomogeneities.[42,47,48] There is also the well-known CE-type charge and spin ordering that has been seen at $x=0.5$ in some of the manganites.

In both $Nd_{1-x}Sr_xMnO_3$ and $Pr_{1-x}Sr_xMnO_3$ Kawano *et al.*[21] and Kajimoto *et al.*[22,25] have seen finite-temperature ($T \simeq 150$ K) first-order transitions at $x=0.5$ from a ferromagnetic metal to an insulating AFM *A* phase. Kajimoto *et al.*[25] have also observed that close to the boundary of the FM and *A* phase of $Pr_{1-x}Sr_xMnO_3$, an unusual stripelike charge-order appears along with this weakly first-order transition. This is distinctly different from the staggered charge-ordering of the CE-type state. Moritomo[49] reports a large region of phase separation between FM and CO in the ground state of $(La_{1-z}Nd_z)_{1-x}Ca_xMnO_3$ immediately beyond $x=0.5$ for $z<0.5$.

Very recently, an inhomegeneous mixture of micron-size regions with no net magnetization and FM regions has been seen in electron holography and dark-field imaging in the low-bandwidth system $La_{1-x}Ca_xMnO_3$ at $x=0.5$ (Ref. 38). Moreover, there is charge ordering seen in both regions. These FM-CO coexistence regions are not found to have any AFM order (expected if there were CE phase admixture) within experimental resolution. The ground-state energies of these different phases seem to be very close, leading to a possible first-order phase transition and consequent phase segregation.

Almost all the experiments discussed above consider orbital ordering as the underlying reason for the various magnetic orders observed in the electron-doped regime. The anisotropy of the two e_g orbitals and the nature of overlap integral between them[11,34] make the electronic bands low dimensional. Such anisotropic conduction in turn leads to anisotropic spin exchanges and different magnetic structures. In the *A* phase the kinetic energy (KE) gain of the electrons is maximum when the orbitals form a two-dimensional (2D) band in the *xy* plane and maximize the in-plane ferromagnetic exchange interaction. However, in the *z* direction the AFM superexchange interaction dominates due to the negligible overlap of $d_{x^2-y^2}$ orbitals. In addition, the presence of charge ordering and inhomegeneous or phase-separated states, particularly around the commensurate densities, is suggestive of the vital role of Coulomb interactions in the manganites. The absence of CE phase in the moderate- to large-bandwidth materials imply that the role of Jahn-Teller or static lattice distortions may not be as crucial in the electron-doped regime even in the region close to $x=0.5$.[80] A model, for the electron-doped systems, therefore, should have as its primary ingredients the two e_g orbitals at each Mn site and the anisotropy of hopping between them. In addition, the Coulomb interactions are present, and their effects on the charge, orbital, and magnetic order are important.[5,30,40,50] In the next section, we use a model recently proposed by van den Brink and Khomskii[51] for the electron-doped manganites and later extended by us[50] in order to take into account the effects of local Coulomb interactions present in these systems. We extend this model further in the present work, study the magnetic and orbital orders in more detail, investigate the possibility of charge ordering and phase separation, and discuss their consequences. In Secs. II and III we present our calculations and results and compare them with experimental literature. We conclude with a brief discussion on the implications of our results.

II. MODEL AND RESULTS

A. Degenerate double-exchange model

Evidently the physics of the region $x>0.5$ is quite different from that in the $x<0.5$ for the manganites and one has to look at the electron-doped manganites from a different perspective. In order to pay due heed to the compelling experimental and theoretical evidence in support of the vital role of the orbitals, van den Brink and Khomskii[51] (BK) have proposed a model for the electron-doped manganites that incorporates the e_g orbitals and the anisotropic hopping between them. In the undoped $LaMnO_3$ compound each Mn ion has one electron and acts as a Jahn-Teller center, the e_g orbitals are split, and the system is orbitally ordered. Thus for the lightly (hole-)doped system one can at the first approximation ignore the orbital degrees of freedom and apply a single-band model like the conventional double-exchange (DE) model to describe it.

In the doped manganites $R_{1-x}A_xMnO_3$ there are $y=1-x$ electrons in the two e_g orbitals at each Mn site and hence the actual filling (electron density) is $y/4$. This means that the highest filling in the electron-doped region is only $\frac{1}{8}$ (we restrict ourselves to $0.5 \leqslant x \leqslant 1.0$ in the foregoing). Due to this low electron concentration and hence very few Jahn-Teller centers, the e_g band is mostly degenerate and the Jahn-Teller effect is negligible to a leading approximation. Neglect of the Jahn-Teller effect is also justified from the experimental evidence presented above. The usual charge and spin dynamics of the conventional DE model then operate here too, albeit with an additional degree of freedom coming from the degenerate set of e_g orbitals. This process has been described by BK as *double exchange via degenerate orbitals*.

In order to capture the magnetic phases properly, the model includes the superexchange (SE) coupling between neighboring t_{2g} spins. At $x=1$ the e_g band is completely empty and the physics is governed entirely by the antiferromagnetic exchange between the t_{2g} spins at neighboring sites. On doping, the band begins to fill up, and the KE of electrons in the degenerate e_g levels along with the attendant Hund's coupling between t_{2g} and e_g spins begin to compete with the antiferromagnetic SE interaction, leading to a rich variety of magnetic and orbital structures. The model used to describe the ground states of the electron-doped manganites is thus

$$H = J_{AF}\sum_{\langle ij\rangle} \mathbf{S}_i\cdot\mathbf{S}_j - J_H\sum_i \mathbf{S}_i\cdot\mathbf{s}_i - \sum_{\langle ij\rangle\sigma,\alpha,\beta} t_{i,j}^{\alpha\beta} c_{i,\alpha,\sigma}^{\dagger} c_{j,\beta,\sigma}. \tag{1}$$

α,β take values 1 and 2 for $d_{x^2-y^2}$ and $d_{3z^2-r^2}$ orbitals and the hopping matrix elements are determined by the symmetry of e_g orbitals.[11,34] Although similar in appearance to the conventional DE model, the presence of orbital degeneracy together with the very anisotropic hopping matrix elements $t_{ij}^{\alpha\beta}$ makes this model and its outcome very different.[4,52,53]

BK treated the t_{2g} spins classically and the Hund's coupling was set to infinity. Canting was introduced through the effective hopping matrix elements[4] $t_{xy}=t\cos(\theta_{xy}/2)$ and $t_z=t\cos(\theta_z/2)$ where θ_{xy} and θ_z are near-neighbor angles between t_{2g} spins in the *xy* plane and *z* direction. The SE energy per state becomes $E_{SE}=(J_{AF}S_0^2/2)(2\cos\theta_{xy}+\cos\theta_z)$. In this level of approximation, the problem reduces to solving the 2×2 matrix equation $||t_{\alpha\beta}-\epsilon\delta_{\alpha\beta}||=0$ for a system of spinless fermions:

$$t_{11} = -2t_{xy}(\cos k_x+\cos k_y), \tag{2a}$$

$$t_{12}=t_{21}=-\frac{2}{\sqrt{3}}t_{xy}(\cos k_x-\cos k_y), \tag{2b}$$

$$t_{22}=-\frac{2}{3}t_{xy}(\cos k_x+\cos k_y)-\frac{8}{3}t_z\cos k_z. \tag{2c}$$

Here t_{11} is the dispersion due to the overlap between $d_{x^2-y^2}$ orbitals on neighboring sites, t_{12} between a $d_{x^2-y^2}$ and a $d_{3z^2-r^2}$ orbital, and t_{22} between two $d_{3z^2-r^2}$ orbitals. In the foregoing, the system is assumed to posses a cubic unit cell. In the doping range considered, the deviations from cubic symmetry are small.[3] For $J_H\to\infty$, writing t_{xy} and t_z in terms of θ_{xy} and θ_z the matrix equation is easily solved to get the energy bands $\epsilon_{\pm}(k)$ as

$$\epsilon_{\pm}(k) = -\frac{4t_{xy}}{3}(\cos k_x+\cos k_y)-\frac{4t_z}{3}\cos k_z \pm \left(\left[\frac{2t_{xy}}{3}(\cos k_x+\cos k_y)-\frac{4t_z}{3}\cos k_z\right]^2+\frac{4t_{xy}^2}{3}(\cos k_x-\cos k_y)^2\right)^{1/2}. \tag{3}$$

In the pure (uncanted) phases the bands in the *A* and *C* phases become purely two and one dimensional. However, even in the presence of canting there is almost no dispersion in the *xy* (*C*-phase) or *z* (*A*-phase) direction. The total energy (band energy$+E_{SE}$) at a particular filling is then minimized with respect to θ_{xy} and θ_z. The sequence of phases follows from the nature of the density of states (DOS) modulated by the anisotropic overlap of orbitals as well as the DE mechanism. Quite remarkably the phase diagram has the sequence of almost all the magnetic phases observed in these systems for $x>0.5$, although it has its own shortcomings. At very low electron doping ($1>x>0.97$) a canted *A*-type AFM phase is obtained[54] which is stable for all values of J_{AF} whereas experimentally a *G*-type antiferromagnetic phase is observed in this range. The other problem is that of the limiting behavior. When the AFM exchange interaction is close to zero (i.e., $t/J_{AF}\to\infty$) the system should be completely ferromagnetic, missed out in their phase diagram.

The limit of infinite Hund's coupling which BK worked with is unphysical for the manganites considered.[3,5,40,55] Typical values reported in the experiments[3,18] and various model studies[5,30,55] and LDA calculations[40,56] do not suggest the spin splittings of the e_g band in various manganites to be very large. These are typically comparable to (or slightly larger than) the e_g bandwidth. The scale of Coulomb correlations is most likely to be even higher.[3,5] The other consequence of using such large Hund's coupling is that the low-energy excitations (like optical spectra, specific heat, spin fluctuation energy scales) are going to be inaccurate and, as we show below, estimates for canting will be too large. BK's calculation, though, serves as an useful starting point for improved theories. In a more realistic treatment of the spin degrees, Pai[57] considered the limit of finite J_H and succeeded in recovering the *G* and *F* phases. From these studies it was also clear that the Jahn-Teller (JT) effect does not play a major role in this region of doping.

B. Double exchange and correlation

We mentioned earlier that by all estimates the Coulomb correlations in these systems are large[19,56,58] and it is not *a priori* obvious, therefore, that the phase diagram obtained by BK will survive once these are introduced. Neither of the treatments of BK or Pai includes the interactions present in the system—namely, the interorbital and intraorbital Coulomb interactions as well as the longer-range Coulomb interactions. Although for low doping the local correlations are expected to be ineffective, with an increase in doping they preferentially enhance the orbital ordering.[50] This affects the F phase and alters the relative stability of the *A* and *C* phases. The longer-range part of the interactions would tend to localize the carriers and lead to charge ordering. It is, therefore, necessary to include them in the Hamiltonian and look for their effects on the phase diagram. The addition of the correlation terms makes the model very different from the ones considered by BK and Pai. Besides, the physics of charge and orbital ordering is beyond the scope of the models earlier considered. The model Hamiltonian we consider consists of two parts; the first part is the same as the Hamiltonian in Eq. (1) we discussed in the previous section. The second part, which is the interaction part, has on-site interorbital and intraorbital interactions and nearest-neighbor Coulomb interaction terms. The total Hamiltonian is therefore

$$H = H_1 + H_{int},$$

where H_1 is the same as in Eq. (1) and

$$H_{int} = U\sum_{i\alpha}\hat{n}_{i\alpha\uparrow}\hat{n}_{i\alpha\downarrow} + U'\sum_{i\sigma\sigma'}\hat{n}_{i1\sigma}\hat{n}_{i2\sigma'} + V\sum_{\langle ij\rangle}\hat{n}_i\hat{n}_j. \tag{4}$$

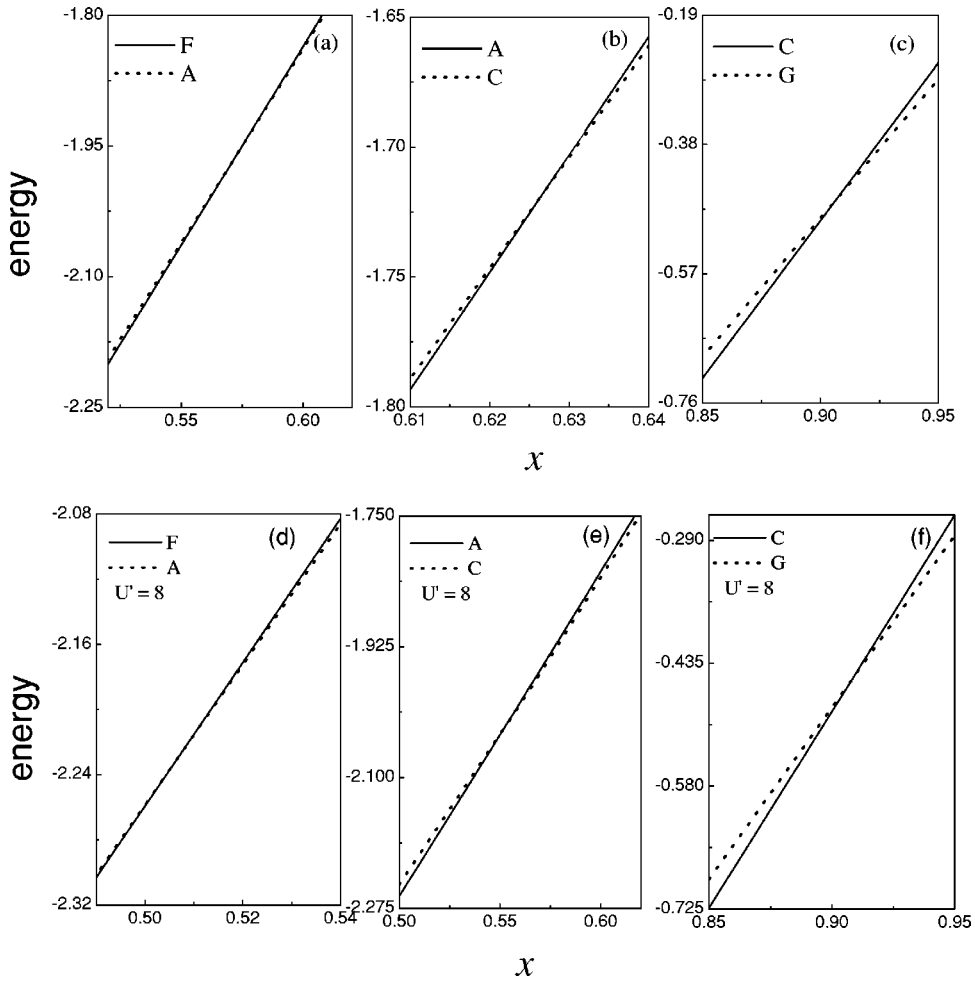

FIG. 2. Ground-state energy of different magnetic phases vs hole concentration $x>0.5$ close to the respective transitions [F phase to A phase in (a), A–C in (b), and C–G in (c)] for $J_H S_0=16.0$ and $J_{AF}S_0^2=0.05$. (d)–(f) show the same in the presence of on-site interorbital Coulomb interaction U'. All energies are measured in units of hopping t.

In the above U, U', and V are the intraorbital and interorbital and the nearest-neighbor Coulomb interaction strengths, respectively. We treat the t_{2g} spin subsystem quasiclassically as in BK, but we work in the more realistic limit of finite values of J_H. In an uncanted homogeneous ground state we choose $\mathbf{S}=\mathbf{S}_0\exp(i\mathbf{Q}\cdot\mathbf{r})$ where the choice of $\mathbf{Q}$ determines the different spin arrangements for the t_{2g} spins.[50] In the infinite-J_H limit, the e_g electron spins are forced to follow the t_{2g} spins, leading to the freezing of their spin degrees of freedom. At finite J_H, however, the quantum nature of the transport allows for fluctuations and the e_g spin degrees of freedom, along with anisotropic hopping across the two orbitals, play a central role. For canted magnetic structures where the angle between two nearest-neighbor t_{2g} spins is different from that of the pure phases, $\mathbf{S}_i$ is given by $\mathbf{S}_i=S_0(\sin\theta_i,0,\cos\theta_i)$ with θ_i taking all values between 0 and π. We will discuss the canted structures at length in the foregoing. We begin our discussion by considering the model without the interaction terms U, U', and V. The interactions and their effects will be dealt with in detail later.

C. Noninteracting limit

Using the usual semiclassical approximation for the t_{2g} spins and the choice $\mathbf{S}=\mathbf{S}_0\exp(i\mathbf{Q}\cdot\mathbf{r})$, the Hamiltonian (1) reduces to

$$H=\sum_{\mathbf{k},\alpha,\beta,\sigma}\epsilon_{\mathbf{k}}^{\alpha\beta}c_{\mathbf{k}\alpha\sigma}^{\dagger}c_{\mathbf{k}\beta\sigma}-J_H S_0\sum_{\mathbf{k},\alpha}c_{\mathbf{k}\alpha\uparrow}^{\dagger}c_{\mathbf{k}+\mathbf{Q}\alpha\uparrow}+J_H S_0\sum_{\mathbf{k},\alpha}c_{\mathbf{k}\alpha\downarrow}^{\dagger}c_{\mathbf{k}+\mathbf{Q}\alpha\downarrow}, \quad (5)$$

where we follow the notation in Refs. 11 and 51. Here $\epsilon_{\mathbf{k}}^{\alpha\beta}$ are the same as $t^{\alpha\beta}$ of Eq. (3).

We can see from the above Hamiltonian that the matrix is now an 8×8 one with two spins (up and down), two degenerate orbitals ($d_{x^2-y^2}$ and $d_{3z^2-r^2}$) with (anisotropic) hopping between them, and two momentum indices ($\mathbf{k}$ and $\mathbf{k+Q}$). Thus, a finite J_H makes the problem a 8×8 one at each $\mathbf{k}$ point in contrast to the 2×2 spinless problem for infinite J_H. The SE part of the ground-state energy is the classical contribution E_{SE}.

We diagonalize the Hamiltonian in Eq. (6) at each $\mathbf{k}$ point on a finite-momentum grid.[50] The ground-state energy is calculated for different magnetic structures (F, A, C, and G) in their uncanted configurations. The magnetic structure with minimum ground state energy is determined for each set of parameters (x, J_H, and J_{AF}) for the entire range of electron doping ($0.5\leqslant x\leqslant1$). In Fig. 2 we show the ground-state energies for different magnetic structures for $J_{AF}S_0^2=0.05$ and $J_H S_0=16$ around the transition points in the doping range

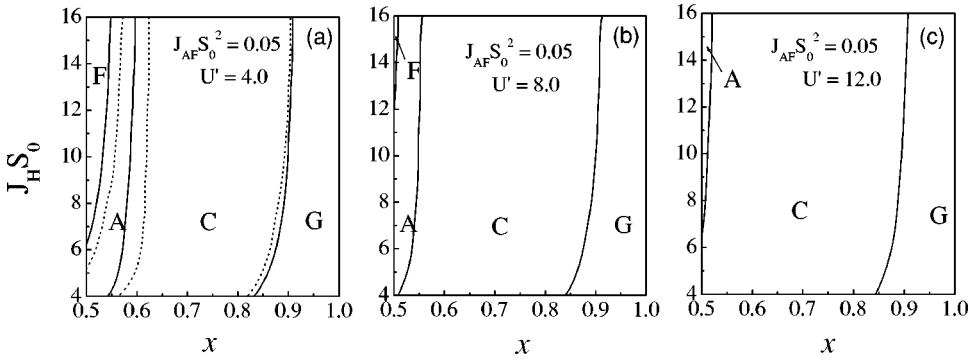

FIG. 3. Magnetic phase diagram in the doping (x)-$J_H S_0$ plane for different U'. Note the gradual shrinking of the F phase in the region $x>0.5$. For low U' the size of the A phase remains unaffected but at larger U' it rapidly shrinks. The C phase grows a bit while the G phase remains nearly unaffected. In (a) the dotted line shows the phase diagram in the absence of U'.

$0.5 \leqslant x \leqslant 1.0$. The value of $J_H S_0$ is chosen somewhat large to compare the figure with $U' \neq 0$ case.[82] All energies are measured in units of t. The figure shows that there is a G-type AFM to C-type AFM transition occurring at $x=0.91$, C-type to A-type transition at $x=0.62$, and A-type AFM to FM (ferromagnet) transition at $x=0.57$. The procedure is repeated for many different values of J_{AF} and J_H to generate the full phase diagrams.

D. Magnetic phase diagram and canting

The phase diagram in the x-$J_H S_0$ plane for a typical value of $J_{AF} S_0^2 = 0.05$ is shown in Fig. 3(a) (dotted lines). In Fig. 4 is shown the phase diagram (dashed line) in the x-$J_{AF} S_0^2$ plane. There is no general agreement on the values of the different parameters involved in manganites. From photoemission and optical studies[5] and local density approximation (LDA) analysis[56] one can glean a range of typical values[40] $0.1\ \text{eV} < t < 0.3\ \text{eV}$, $J_H \simeq 1.5$–2 eV, and $J_{AF} \simeq 0.03t - 0.01t$ (Ref. 59). We observe that for low values of $J_H S_0$, an A-type AFM phase is stable near $x=0.5$, then the C phase is stabilized for a wide region in the intermediate doping range, and finally near $x=1$ the G-type AFM phase has the lowest energy. For higher values of $J_H S_0$ the FM phase has the lowest energy near $x=0.5$ and the sequence of magnetic phases from $x=0.5$ to $x=1$ is $F \rightarrow A \rightarrow C \rightarrow G$. All the transitions appear to be continuous without any jump in the magnetic order parameters. The general trend observed here is in good accordance with the experimental phase diagram of the electron-doped manganites of intermediate bandwidth such as $Nd_{1-x}Sr_xMnO_3$ and $Pr_{1-x}Sr_xMnO_3$ (Refs. 22, 24, and 25).

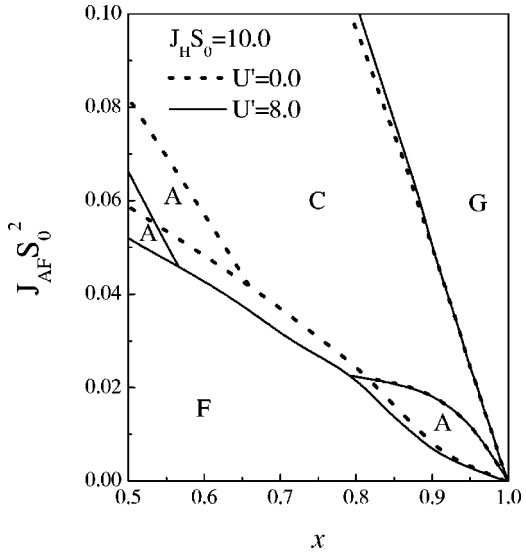

FIG. 4. Magnetic phase diagram in the doping (x)-$J_{AF} S_0^2$ plane with $U'=0$ and 8.

At low electron doping the SE still wins over the KE gain of the electrons via the development of a ferromagnetic component of spins in the DE mechanism. Thus the G phase is stable up to a finite electron doping. The value of x where the G phase becomes unstable depends weakly on J_H in the experimentally relevant region. The KE is an increasing function of doping and for small doping it is proportional to the (electron) filling whereas the SE energy is nearly independent of x (Ref. 60). A three-dimensional AF spin alignment such as G phase does not allow delocalization of electrons for the typical values of J_H. To gain KE the system tries to polarize the spins along one, two, and finally all three directions successively in the sequence C, A, and F phases. Thus the C-type AFM phase with ferromagnetically aligned spins along the z direction appears first as we increase the electron doping. Then appears the A-type AFM phase with a two-dimensional spin alignment and finally the FM phase is observed.

The stability of A and C phases is further enhanced by the ordering of orbitals in these phases. As we show below, the A phase has an orbital ordering of $d_{x^2-y^2}$ type and the C phase $d_{3z^2-r^2}$ type. The planar $d_{x^2-y^2}$ orbital order in the xy plane in the A phase and rodlike $d_{3z^2-r^2}$ orbital order in the z direction in the C phase facilitate the hopping of electrons (along the plane for A phase and across it for the C phase). Hence, it is primarily the orbital order that regulates the DE mechanism and leads to the C- and A-type magnetic orders. Such a scenario has been borne out in several experiments[20,22,35] where evidence for orbital ordering is seen at a much higher temperature than the spin ordering. However, in the G and F phases no significant orbital ordering has been observed. Thus the interplay of spin alignment along chains or planes and the corresponding orbital order lead to the transformation from the one-dimensional to the two-dimensional and finally to the three-dimensional magnetic structure with increased doping. The competition between effective KE (determined by J_H, band filling, and orbital ordering) and SE leads to the transitions $G \rightarrow C \rightarrow A \rightarrow F$ (with the number of antiferromagnetic bonds 6, 4, 2,

and 0 per site, respectively) as the doping is varied. The dimensionality of the magnetic and orbital order in the *A* and *C* phases described above is reflected in the DOS in these phases. In the *A*-type AFM phase the dispersion of bands is two dimensional with a peak near the center of the band and small but nonzero DOS at the band edges when the hopping t_{12} is zero. For a finite t_{12} the peak at the center of the DOS splits. In the canted *C* phase the DOS is quasi one dimensional (for $t_{xy}=0$ it becomes purely one dimensional) with peaks towards the band edges.

Experimentally[20,22] it is observed that there is little canting in *A* and *C* phases in most of these systems. There are some experimental observations[61] on $Sm_{1-x}Ca_xMnO_3$ which suggest that the *G* phase, for low doping, has small canting. Canting of the core spins is included in our calculation by writing $\mathbf{S}_i=\mathbf{S}_0(\sin\theta_i,0,\cos\theta_i)$ in the Hamiltonian with θ_i taking values between 0 and π. Such a canted spin configuration connects two different spin species (up and down) at the same site. With this choice of $\mathbf{S}_i$, the Hund's coupling term between t_{2g} and e_g spins in the Hamiltonian becomes

$$H_{Hund}=-J_HS_0\sum_{i,\alpha}\cos\theta_i(c^\dagger_{i\alpha\uparrow}c_{i\alpha\uparrow}-c^\dagger_{i\alpha\downarrow}c_{i\alpha\downarrow})$$

$$-J_HS_0\sum_{i,\alpha}\sin\theta_i(c^\dagger_{i\alpha\uparrow}c_{i\alpha\downarrow}+c^\dagger_{i\alpha\downarrow}c_{i\alpha\uparrow}).$$

In the case of canted magnetic structures the different magnetic phases need to be defined at the outset. The convention to define the magnetic phases are the following: The phase is *A* type when $\theta_{xy}<\theta_z$ as the spins in the *xy* plane have more ferromagnetic component than the spins across the planes. Similarly, in the *C* phase $\theta_{xy}>\theta_z$. In the canted *G* and *F* phases both angles θ_{xy} and θ_z are close to 180° and 0°, respectively. The qualitative nature of the phase diagram is very similar to the uncanted phase diagram except for little shifts in the phase boundaries (the shifts are small unless J_H is large). We show in Fig. 5 the angle of canting as a function of J_H deep inside the *G* phase at $x=0.98$ (the angles in Fig. 5 represent the deviation from 180°) for different values of $J_{AF}S_0^2$.

There is almost no canting in the *z* direction while in the *xy* plane there is insignificant canting for low J_H and it is about 10° only for large J_H. The absence of canting in θ_z is seen for all different values of $J_{AF}S_0^2$. An increase in J_{AF} reduces the canting of θ_{xy} (Fig. 5, inset) and stabilizes the pure *G* phase as expected. Changing *y* and moving closer to the boundary with the *C* phase, canting in θ_{xy} is seen to increase quite slowly. However, very close to the *G*-*C* boundary, θ_{xy} reverts back towards π while θ_z begins to deviate from π. On doping, the delocalization of electrons is costly in a purely AFM configuration (J_H being the largest scale) and the spins will begin to cant. The canting angle will be anisotropic; i.e., θ_z is going to be different from θ_{xy} due to the anisotropy of $t_{ij}^{\alpha\beta}$. We also note that the canting in the plane leads to a higher gain in KE as against canting in the *z* direction. This does not, however, mean that the phase that abuts *G* phase would be the planar (*A*-type) phase; it is in fact the *C* phase that appears first. The magnitudes of the two angles are delicate functions of doping and the dimensionality of the DOS as well as the anisotropy of the hopping integral. The phase that appears after the *G* phase with increased doping is the *C* phase.

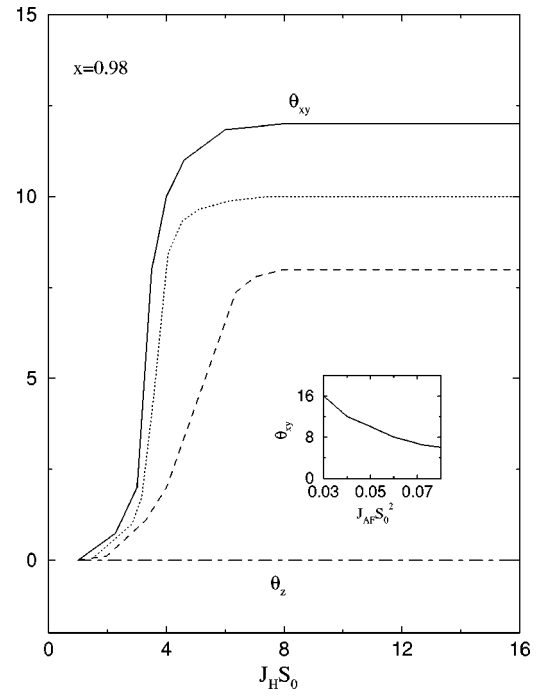

FIG. 5. Canting of the angles θ_{xy} and θz in degrees as a function of J_HS_0 for $J_{AF}S_0^2=0.04$ (solid line), 0.05 (dotted line), and 0.06 (dashed line). θ_{xy} vs $J_{AF}S_0^2$ at $J_HS_0=10$ is shown in the inset.

In the $J_H\rightarrow\infty$ limit the effective hopping is $t\cos(\theta/2)=0$ in an AFM background. Hence on doping canting of the core spins is expected to be large as it leads to the FM component and facilitates hopping from site to site. In the $J_H\rightarrow\infty$ effective theory the ''wrong'' spin sector of the Hilbert space is projected out and canting is large. However, at finite J_H this picture is changed altogether. An electron in the wrong spin state costs a finite energy ($\propto J_H$). Hence the canting angle reduces drastically. In fact, for realistic values of J_H the canting is almost negligible as we see from Fig. 5. Moreover, the KE gain, which is proportional to doping (for small doping), cannot overcome the SE energy unless *x* deviates from 1 reasonably. Hence one gets a canted *G* phase with very small canting angles in the region close to $x=1$, resembling the end-member pure *G* phase. Since the KE contribution is quite small (due to the small values of canting), this phase does not have any preferential orbital arrangement. Evidently the region of *G* phase will grow with an increase in J_{AF}. Conversely, for $J_{AF}\rightarrow 0$ the system should exhibit ferromagnetism for any doping. However, BK find that the phase boundary between the canted *G* phase and the *C* phase does not change significantly as J_{AF} is varied. In contrast, the phase diagram we obtained gives an FM state for $J_{AF}\rightarrow 0$ for the entire doping regime and the stability of the *G* phase grows with J_{AF}.

Using four *Q* vectors it is possible to define a CE-type magnetic order. In the pure degenerate DE model, at finite

J_H, Pai has found this state stable at $x=0.5$. We observe that this state is unstable anywhere away from $x=0.5$ towards A or F phases.[62] Our results agree in general with the results of Maezono *et al.*[63] though the A phase near $x=0.5$ is missing in their work. Solovyev and Terakura[64] studied the noninteracting Hamiltonian of BK in the same $J_H \to \infty$ limit using a multiple-scattering approach. With well-defined conventions for different spin order, they succeeded in recovering the magnetic phases in the x-J_H plane with intermediate regions having significant spin canting. As pointed out by Maezono *et al.*[30] and us[50] earlier, orbital ordering in the A phase forbids KE gain even when there is finite FM component in the z direction. We do not find any significant canting in either the A or C phase (or at their boundaries) and believe that canting in those regions is primarily an artifact of the infinite-J_H approximation and incomplete orbital order discussed above. Besides, any finite Coulomb interaction (U') will enhance the orbital order and reduce canting further. Experimentally, however, there is hardly any evidence for significant canting in those values of x. In a related work, Sheng and Ting[65] considered the problem from the strong correlation point of view in contrast to the band limit that we have adopted. The C phase, however, could not be obtained in their Monte Carlo study in the region $x \geqslant 0.5$.

III. INTERACTING CASE

A. Magnetic phases

We treat the three interaction terms in the Hamiltonian (5) in the mean-field theory. It has been pointed out by Hotta *et al.*,[55] that the mean-field theory for the interacting DE model even in low dimension gives very good agreement with exact diagonalization on small systems. Comparison of mean-field phase diagram with exact diagonalization on small systems by Misra *et al.*[40] is also quite encouraging. We first look into the interorbital Coulomb interaction term $U'\Sigma_{i\sigma\sigma'}\hat{n}_{i1\sigma}\hat{n}_{i2\sigma'}$ and set $U=V=0$. In the mean-field theory, one neglects fluctuations and writes $\hat{n}_{i1\sigma}\hat{n}_{i2\sigma'} = \langle\hat{n}_{1\sigma}\rangle\hat{n}_{i2\sigma'} + \langle\hat{n}_{2\sigma'}\rangle\hat{n}_{i1\sigma} - \langle\hat{n}_{1\sigma}\rangle\langle\hat{n}_{2\sigma'}\rangle$.

The homogeneous averages $\langle\hat{n}_{1\uparrow}\rangle$, $\langle\hat{n}_{1\downarrow}\rangle$, $\langle\hat{n}_{2\uparrow}\rangle$, and $\langle\hat{n}_{1\downarrow}\rangle$ were calculated iteratively through successive diagonalization of the Hamiltonian. Each of the average quantities and the filling were calculated from the resultant eigenvectors for a chosen chemical potential and fed back to the Hamiltonian for next iteration. All the averages and filling were thus allowed to reach self-consistent solutions. Self-consistency is achieved when all averages and the ground-state energy converge to within 0.01% or less (depending on the difference in energy with the competing ground state). In this way the ground-state energies are calculated at each filling for all four magnetic phases (F, A, C, and G) and the minimum-energy phase was determined to obtain the complete magnetic phase diagram in the entire electron-doping regime by varying both J_H and J_{AF}.

We show in Figs. 2(d)–2(f) the ground-state energies of different magnetic phases around the transition points with $J_{AF}S_0^2=0.05$, $J_HS_0=16$, and $U'=8$. The G-C phase transition occurs at $x=0.91$ as in the $U'=0$ case, C-A transition at $x=0.57$, and the A-F transition at $x=0.51$. Comparing this with Figs. 2(a)–2(c) we note the shift of position of the transitions. The G phase remains unaffected, the C phase widens, and F phase shrinks for $U'>0$. The panel from Figs. 3(a)–3(c) show the progression of the phase diagram as U' increases. The $U'=0$ phase diagram is shown in Fig. 3(a) by dashed lines for comparison.

It is observed that on increasing U' the ferromagnetic phase starts shrinking fast, the C phase gains somewhat while the G phase remains almost unaltered for the entire range of values of J_HS_0 studied. The trends observed here are in good agreement with the experimental observations of Kajimoto *et al.*[22,25] and Akimoto *et al.*[20] [see Figs. 1(a) and 1(b)]. The enhanced correlation effectively reduces the phase space for the electrons. The observation[20,25] that on decreasing the bandwidth the ferromagnetic phase shrinks and finally gets pushed below $x=0.5$ with the A phase becoming stable at $x=0.5$ is borne out in Fig. 3. The stabilities of A and C phases are primarily derived from the enhanced orbital ordering in the A and C phases driven by the interorbital repulsion and the low-dimensional nature of the DOS. In the presence of U', the one-dimensional order leading to the AFM instability in the C phase seems to grow faster. Close to the $x=1$ end the electron density is very low; there are almost no sites with both orbitals occupied and U' is therefore ineffective. The G phase remains almost unaffected as seen in Fig. 2. Similarly the canting of the spin away from π observed in the G phase remains the same as in Fig. 5. At the other end, however, the electron density is higher and the F phase has preferential occupation of one species of spin at both the orbitals. Hence this phase is affected drastically by the interorbital repulsion.

We also compare the phase diagrams with and without U' in the x-J_{AF} plane for $J_HS_0=10$. The corresponding phase diagram is shown in Fig. 4. Trends observed in Fig. 3 are also seen in this case. The topology of the phase diagram has not changed much with finite U', though the A phase and F phase shrink in the presence of U' while the C phase has grown.

It is known[55] that at the level of mean-field theory the intraorbital repulsion U between opposite spins mimics the effect of J_H. As we are working with quite low densities (actual filling $\leqslant 0.125$) and the relevant J_H values are moderate to large, there is hardly any site with both spin species. Therefore, we find almost no observable effect of U on the phase diagram (except for very low J_H where again the changes are small) and keep its value zero in the phase diagrams that follow.

B. Magnetic ordering and disorder

The doped manganites $R_{1-x}A_xMnO_3$ are intrinsically disordered owing to the substitution of trivalent ions by divalent ones. Although the dopant ions do not enter the active network of MnO_6 octahedra that are considered central to the transport properties and magnetic ordering, their effects cannot be ignored. In this kind of substitution not only are the charges on the dopant ions different from the trivalent rare-

earth ions they replace, the ionic sizes of the rare earths vary considerably (e.g., La, Nd, and Pr all have different ionic sizes). Hence there is a mismatch of ionic sizes between these and the divalent ion (like Sr, Ca, etc.) that replaces them. Such a mismatch would quite naturally bring about large lattice distortions locally.

However, the effect of disorder has been completely ignored in the treatments discussed so far. BK and Pai[57] argue that to a first approximation, the disorder does not seem to play a major role in the magnetic phase diagram in this region of doping. This is possibly due to the nonmagnetic nature of the disorder—the rare-earth ions are not found to have any observable moment except for Pr and it has been shown that Pr-Mn coupling does not have a detectable effect[66] in the magnetic structure. They, however, considered substitution only at the rare-earth site.

Since the Mn ions are central to the mechanism of magnetic and orbital order in the manganites, substitution at this site would be quite revealing. In the last few years quite a few experimental investigations[67,68] have been carried out by substitution of Mn by Fe, Ga, and Al. These have similar ionic sizes and valences as Mn and therefore cause very little distortion in the lattice.[67] For example, the substitution of Mn^{3+} by Fe^{3+} (which has identical ionic size as Mn^{3+}) in $La_{1-x}Ca_xMn_{1-y}Fe_yO_3$ in the AFM region at $x=0.53$ shows that the resistivity increases and magnetoresistance disappears by about $y=0.13$. Although the Fe^{3+} has a higher moment than the Mn^{3+} that it replaces, one observes a steady suppression of the magnetic moment and ferromagnetism with Fe doping.[67] Whether there is any accompanying changes in the underlying magnetic ordering is not clear. Also the systematics across several manganites with different bandwidths are also not available yet.

There are two things that happen when Fe is doped in place of Mn: (i) In the octahedral crystal field the Fe^{3+} (high-spin d^5 configuration) sites have all their $e_{g\uparrow}$ orbitals filled up and forbid the motion of electrons from Mn^{3+} into Fe^{3+} sites, preventing DE mechanism from operating and (ii) the presence of an Fe^{3+} instead of Mn^{3+} in any site alters the superexchange interaction between this and the neighboring sites. It is possible to account for these effects in a qualitative manner following Alonso *et al.*[69]

The fraction of Mn^{4+} sites (which is the depletion in the number of electrons in the system) is increased by $(1-y)^{-1}$ when $y\neq 0$ as compared to $y=0$. For the range of y, Ahn *et al.*[67] work with ($y\sim 0.10$), this is only about 10%. So the effective depletion of electrons and effect (i) can be neglected to a first approximation deep inside any given phase. Similar situation obtains when Al^{3+} or Ga^{3+} (having filled d band) are doped.

The change in the SE interaction is approximated by estimating the change in the effective antiferromagnetic interaction between neighboring core spins owing to the changed values of them in the coupling of Mn-Mn, Mn-Fe, and Fe-Fe. The new (effective) J_{AF} is given by

$$J_{AF}^{eff}=J_{AF}\left[(1-y)^2+\frac{5}{3}2y(1-y)+\frac{25}{9}y^2\right].$$

The prefactors (25/9, 5/3, and 1) come from the new spin values involved and the factors $(1-y)^2$, etc., are for counting the probability of sites with Mn-Mn, Mn-Fe, and Fe-Fe bonds, respectively. Then, at $y=0.12$, for example, the effective J_{AF} is about 0.06 if the initial value of J_{AF} is 0.05. This will enhance the AF tendencies (and can even take the system from the *F*- to *A*-type AFM phase as in Fig. 4 for x close to 0.5) and increase the resistivity as observed by Ahn *et al*.

Although a smaller effect, the depletion of the effective number of electrons taking part in the DE mechanism will reduce the conductivity and move the effective doping x towards right in the phase diagram and increase AF correlations and resistivity further. There is also the possibility that due to these combined effects, the magnetic ground state may get altered, a possibility only further experiments will reveal.

There is another source of scattering coming from the localized t_{2g} spins at each Mn site. The itinerant e_g electrons, in a mean-field sense, can be thought of as moving in a magnetic "field" of the localized spins. It has been shown[70] that such a random field can indeed localize part of the electronic states, particularly in the low-dimensional bands (as obtain in *C* and *A* phases). Substitution of Mn^{3+} by Fe^{3+}, which has a different moment (5/2 as opposed to 2), introduces random changes in this field and additional channel for scattering. The observation[71] of a spin-glass-type phase at low temperature in the Cr-doped $La_{0.46}Sr_{0.54}Mn_{1-y}Cr_yO_3$ ($0<y<0.08$) is a possible indication of how the competing interactions between the coexisting FM phase in the metallic *A*-type AFM matrix is affected by scattering off the random magnetic Cr impurity and the resultant localization of mobile charge carriers.

C. Orbital ordering

In the noninteracting case we observed orbital order in both the *A* phase ($d_{x^2-y^2}$ type) as well as in the *C* phase (of $d_{3z^2-r^2}$ type). Such orbital order is also borne out in experiments discussed above. In the interacting situation, we calculate the orbital occupancies from the eigenvectors corresponding to the converged ground-state solutions for both $d_{x^2-y^2}$ and $d_{3z^2-r^2}$ orbitals in *A* and *C* phases in their respective regions of stability and show the results in Fig. 6. In the *A* phase the $d_{x^2-y^2}$ orbital has a higher occupancy whereas in the *C* phase it is reversed. We check that the sum of the occupancies of the two orbitals is equal to the actual filling in all the phases. The three-dimensional magnetically ordered *F* and *G* phases, however, show no orbital ordering.

The presence of interorbital Coulomb interaction U' enhances the orbital ordering in both *A* and *C* phases as shown in Fig. 6 for three different U'. Note that at lower electron densities—i.e., as x increases—the effect of U' on the orbital occupancies becomes less pronounced and the curves for different U' merge as expected. We also note that the effect of U' is noticeable in both the *A* and *C* phases. The orbital densities in the *C* phase attain their saturation values by $U'\simeq 8$. Since we are interested in the region $x\geqslant 0.5$, we have not plotted the orbital densities in the *A* phase beyond U'

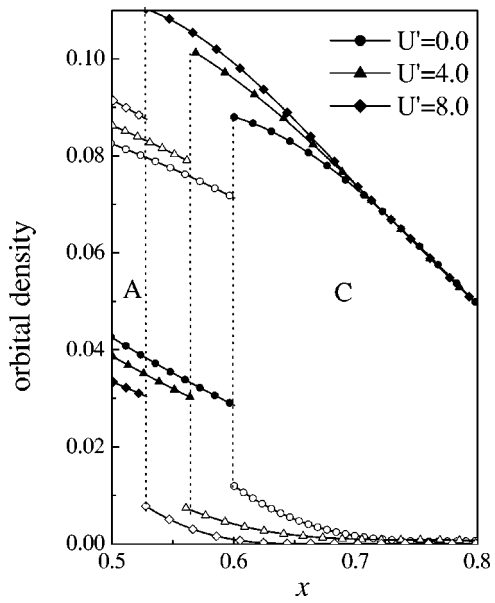

FIG. 6. Orbital densities as a function of doping x for three values of $U'=0$, 4, 8. The solid symbols are for d_{z^2} and open symbols for $d_{x^2-y^2}$ orbitals. The vertical dotted lines represent the boundary between A and C phases for different U'. We choose $J_H S_0=5$ here in order to have stable A and C phases for a reasonable range of x (see Fig. 3) for all three U' values. $J_{AF}S_0^2$ was kept at 0.05.

$=8$—above this value the A phase shifts below $x=0.5$ at $J_H S_0=5$. In the large U' limit the Hamiltonian can be mapped onto a pseudospin Hubbard model[19,72] with off-diagonal hopping [which breaks the SU(2), while still retaining the global U(1) symmetry]. Such a model overestimates the orbital order[72] and the orbital-paramagnetic state is almost never obtained.

The orbital order obtained in the A and C phases leads to anisotropic band structures in these phases and this feature becomes sharper as J_H increases. In particular, the C phase has a quasi-one-dimensional density of states. Ideally, this phase should be conducting in the z direction along the ferromagnetic chains while insulating in the plane. However, experimentally one finds this phase to be nonmetallic. The nearly one-dimensional nature of transport makes it very sensitive to disorder, possibly localizing the states. In the A phase the nature of the occupied orbitals impedes electron motion along the z direction, giving rise to a large anisotropy between the in-plane and out-of-plane resistivities.[25] Therefore the A phase with its planar ferromagnetic alignment (and quasi-2D DOS) is less sensitive to disorder and exhibits in-plane metallic behavior.[20,24,25]

D. Charge ordering

The nearest-neighbor Coulomb interaction term $V\Sigma_{\langle ij\rangle}\hat{n}_i\hat{n}_j$ is also treated in the mean-field theory with $\langle\hat{n}_i\rangle = n + C_0\exp(i\mathbf{Q}\cdot\mathbf{r}_i)$ where C_0 is the charge-order parameter, n is the average number of electrons per site, and $\mathbf{Q}=(\pi,\pi,\pi)$. We calculate the charge-order parameter C_0 self-consistently. Keeping $U'=0$, the major change observed in the phase diagram now is the absence of the A phase and the presence of charge ordering for values of $V>0.29$. The typical values of V are between 0.2 and 0.5 (Refs. 3 and 5) (in units of t). Below $V=0.29$, we do not observe any charge ordering and the A phase reappears. The phase diagrams in the x-$J_H S_0$ plane are shown in Figs. 7(a)–7(c) with $V=0.4$, $V=0.5$, and $V=0.6$ at $U'=0$. Note that there are only three phases now. A coexisting ferromagnetic and charge-ordered (F-CO) phase, the orbitally ordered C phase, and the G phase. The topology does not change appreciably when U' is finite. The resultant phase diagram is shown in Fig. 8. The pattern reflects what is seen in Figs. 3(a)–3(c). The F-CO phase reduces while the C phase grows slightly with U'.

In Figs. 7 and 8 a wide region of F-CO phase is observed near $x=0.5$. This observation is somewhat reminiscent of the recent experiments[20,25] where the charge-ordered phase close to $x=0.5$ is possibly residing at the boundary of the F and A phases and straddling both. Such F-CO phase coexistence is also seen by Moritomo[49] in Nd-substituted $La_{1-x}Ca_xMnO_3$. As noted earlier, grains of F-CO coexistence at $x=0.5$ in $La_{1-x}Ca_xMnO_3$ have been observed recently,[38] although the coexisting F-CO region that we get is considerably wider. We do not find any self-consistent solution with both the A phase and charge ordering for any V. It is possible that the charge ordering instability is too strong close to commensurate ($x=0.5$) filling. The A phase, being also close to $x=0.5$ and deriving its stability from a low-dimensional DOS, gets affected by the charge-order instabil-

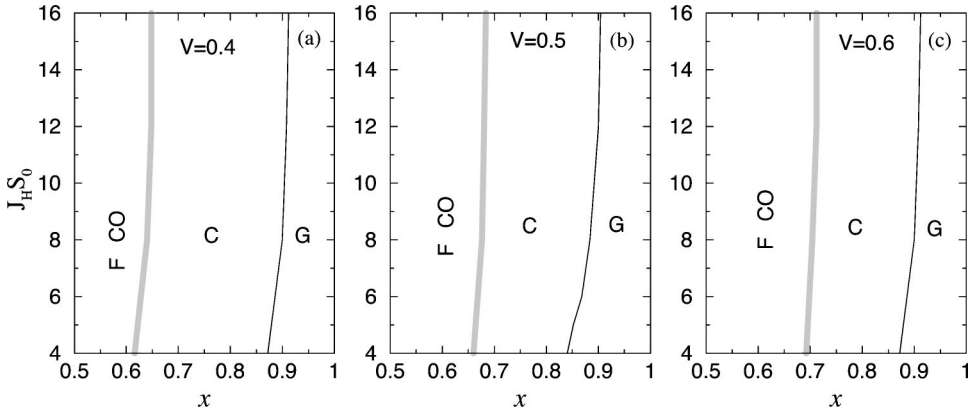

FIG. 7. Magnetic phase diagram in the doping (x)-$J_H S_0$ plane for three different V. The F-CO region gets wider with increasing V. The F-CO to C transition is first order and shown with hatching while others are continuous as in Fig. 3.

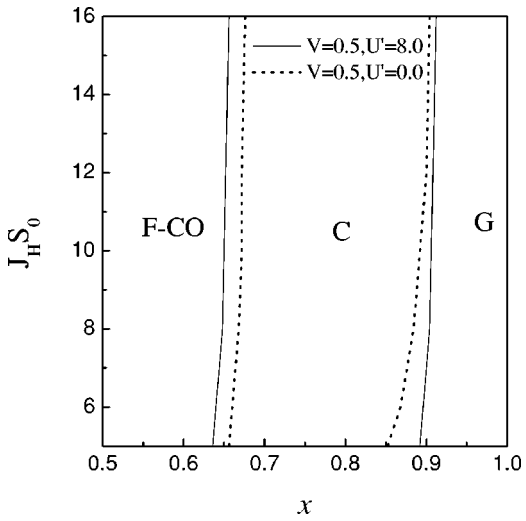

FIG. 8. Magnetic phase diagram in the doping (x)-$J_H S_0$ plane for finite V at two different values of U'. Note that on changing U' the trend follows that in Fig. 3. The F-CO to C transition is not hatched here to show the effect of changing U'.

ity. Both C and G phases are seen to have no charge ordering in them. Unlike in the CE phase, the CO state obtained here has staggered charge ordering in all directions.

Our observation of the ferromagnetic charge-ordered (F-CO) ground state agrees qualitatively with the mean-field calculation of Jackeli *et al.*[73] They considered a Hamiltonian that has orbital degeneracy, Hund's exchange, superexchange, and the near-neighbor Coulomb term and studied the ground-state phase diagram as V and J_{AF} change. There is no local Coulomb term in their model. They restrict their calculations to the $x=0.5$ and $J_H \rightarrow \infty$ limit only and obtained charge-ordered F, A, C, and G phases in the $J_{AF}S_0^2$-V plane when the degeneracy of the e_g orbitals is neglected. In the degenerate model, the F-CO phase appears only at a critical value of $V \approx 0.7$. There is no A phase until $J_{AF}S_0^2$ reaches 0.1. All the transitions from the F-CO phase into AFM states are first order.

We do indeed find a critical value of V for the F-CO phase to appear. The critical value of V for $J_H S_0 = 8$ and $J_{AF}S_0^2 = 0.05$ at $x=0.5$ is about 0.3, well below the value at the $J_H \rightarrow \infty$ limit. The larger value of critical V is an artifact of the $J_H \rightarrow \infty$ limit. The tendency to large canting away from pure AFM spin structures is markedly reduced in the finite-J_H limit as we discussed above. The infinite-J_H limit is, therefore, expected to overestimate the critical value of the near-neighbor repulsion responsible for CO instability in this model as the canting and eventual ferromagnetic instability with a uniform charge distribution are too strong in that limit. This critical value is nearly independent of x inside the region of stability of the F-CO phase for the parameter values we considered. This is an indication of a possible phase separation (with first-order transition) with part of the system pinned at the commensurate density. The CO order parameter C_0 has a discontinuous jump at the transition from the C phase into the F-CO phase as shown in Fig. 9(a), which is a signature of a first-order transition between two states having different magnetic symmetry. A similar first-order jump has been seen at in previous work[40,73] as well and borne out in several experiments described above. The transition as a function of V from pure F to F-CO phase appears to be continuous [Fig. 9(b)].

IV. DISCUSSION

A summary of the trends observed as a function of near-neighbor interaction U' across the entire range of electron doping is presented in Fig. 10. A comparison with Fig. 1(a) reveals the similarity between them if one interprets the increase in U' as an effective reduction in the mobility of electrons and suppression of the DE mechanism. The rapid reduction in the stability of F and A phases at large U' and an almost unchanged G phase are indeed observed in Fig. 1. The C phase is stable over a wider region of phase diagram in Fig. 10 than what is experimentally observed.

There are several appealing features of the model and the limits that we have studied in the present investigation. We have been able to show that the phase diagram and orbital ordering resemble the experimentally observed ones for the electron-doped regime to a large degree. By putting in correlations the orbital orders are enhanced and it was possible

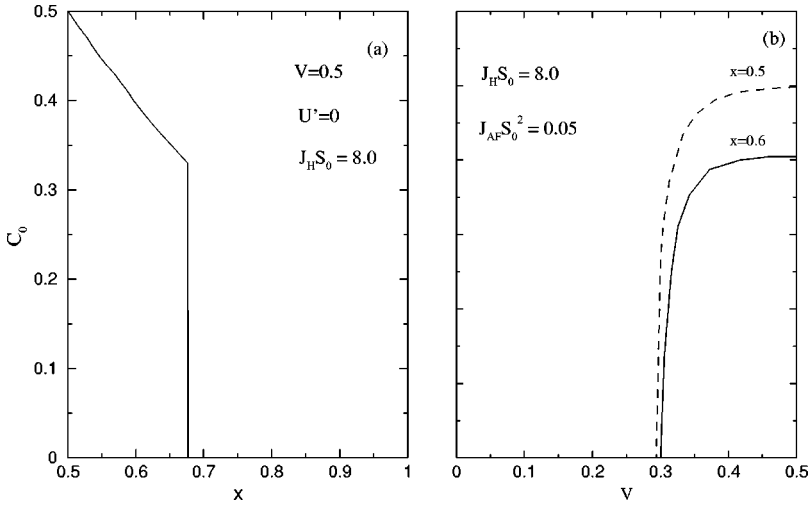

FIG. 9. (a) The charge-order parameter vs hole concentration for $J_{AF}S_0^2 = 0.05$ and (b) the same vs V for two different dopings. The transition F to F-CO as a function of V is continuous.

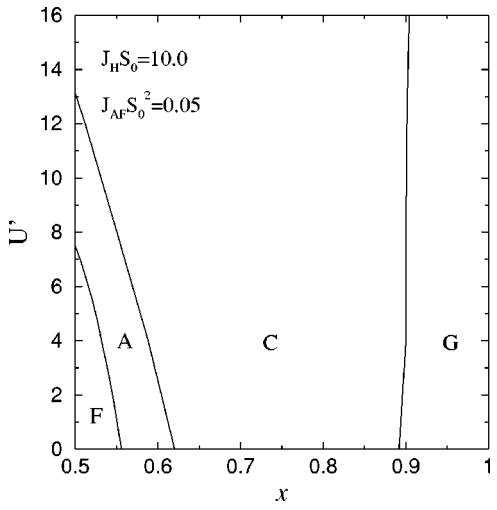

FIG. 10. Summary of the general trend observed in the various phase diagrams (for $V=0$). Note the trend with increasing U' follows closely that of Fig. 1(a) with decreasing bandwidth.

to obtain regions of charge ordering close to $x=0.5$. However, there are several interesting questions that need to be addressed. The neglect of Jahn-Teller effects may well describe the electron-doped manganites in the moderate- to large-bandwidth systems and also works for low-bandwidth systems at low electron doping. But the presence of CE-type ordering at $x=0.5$ in the entire class of low-bandwidth materials reminds us that the effects are relevant close to this doping. A more complete theory should account for the Jahn-Teller distorted Mn^{3+} sites and evolve from the low-bandwidth to the large-bandwidth description successfully. Such a theory, however, is lacking at present.[74]

The region close to $x=0.5$ has a lot of competing states and a large body of literature exists on the first-order transitions and coexisting phases or phase separations into competing orders in this region. The model described here gives a first-order transition from an *F*-CO state to a *C*-type AFM state with concomitant phase separation, albeit with a large region of stability for the CO state. In real systems, with longer-range Coulomb interactions present, the phase separation is likely to appear as domains of one phase dispersed in another. Whether this indeed is the mechanism of the inhomogeneous phases observed or they are intrinsic to the systems[41,42,47,74] is an open question. Transport properties in this region are going to be intriguing with possible percolative growth of FM clusters in an applied magnetic field as an alternate route to negative magnetoresistance as opposed to the DE mechanism.

Extending the model we considered with the possible inclusion of lattice degrees of freedom and from a finite-temperature calculation, it should be possible to look into stripe formations and anisotropic charge orders. It has been suggested[75] recently from a finite-temperature mean-field calculation with a degenerate, noninteracting DE model at the infinite-J_H limit that without the Jahn-Teller physics brought in, the CE phase at $x=0.5$ in the low-bandwidth system is not accessible, though the possibility is wide open[33] in the presence of Coulomb interactions like U' and V.

There is a major class of layered manganites for which the electron-doped side is still unexplored in detail. The bilayer systems like $La_{2-2x}Sr_{1+2x}Mn_2O_7$ have shown[76] similar anisotropic magnetic structures as in 3D manganites. Preliminary results from a mean-field analysis[77] show interesting promise. It is difficult though to account for the large region of *C*-type ordering seen in experiments in such layered systems at doping (x) ranges as high as 0.75–0.90. In the layered systems the DE mechanism is expected to favor either a planar *A*-type or a *G*-type state, depending on the carrier concentration, over the 1D *C*-like ordering.[81] The present model may need additional inputs like coupling to distortions in the lattice in order to understand the layered manganites.

We have not looked into the excitation spectrum of the manganites so far. The effects of fluctuation coming from both spin and orbital degree and their coupling may lead to complicated excitations.[19,29,78] They will affect the thermodynamics quite strongly. The controlled incorporation of disorder, particularly without affecting the lattice[67,68], has opened up a host of possibilities. The observation of nonmetallic behavior in an inhomogeneous mixture of two metallic phases[39] is an indication of the complex nature of coupling across the boundary of such domains. The spin-glass-like phase reported close to the border of the hole- and electron-doped region[71] in $La_{0.46}Sr_{0.54}Mn_{1-y}Cr_yO_3$ is another manifestation of the complicated coupling of the impurity with spin and charge degrees of freedom. More results of such impurity doping in the electron-doped manganites are expected in the near future. We have extended the model we used to incorporate some of these effects[79] and it would be quite instructive to investigate the nature of coupling between the impurity and the magnetic and orbital degrees of freedom.[80–82]

ACKNOWLEDGMENTS

The research of A.T. has been funded by a grant from the Department of Science and Technology, government of India. We acknowledge several useful discussions with S. D. Mahanti and G. V. Pai. Discussions with S. K. Ghatak and Rahul Pandit are also acknowledged.

*Electronic address: tulika@mpipks-dresden.mpg.de
†Electronic address: arghya@phy.iitkgp.ernet.in, arghya@cts.iitkgp.ernet.in

[1] *Physics of Manganites*, edited by T.A. Kaplan and S.D. Mahanty (Kluwer Academic, New York, 1999).
[2] Y. Tokura, *Colossal Magnetoresistive Oxides* (Gordon and Breach, New York, 2000).
[3] J.M.D. Coey, M. Viret, and S. von Molnar, Adv. Phys. **48**, 167 (1999).
[4] C. Zener, Phys. Rev. **82**, 403 (1951); P.G. de Gennes, *ibid.* **118**, 141 (1960); P.W. Anderson and H. Hasegawa, *ibid.* **100**, 675 (1955).

[5] E. Dagotto, T. Hotta, and A. Moreo, Phys. Rep. **344**, 1 (2001).
[6] A.J. Millis, P.B. Littlewood, and B.I. Shraiman, Phys. Rev. Lett. **74**, 5144 (1995); A.J. Millis, B.I. Shraiman, and R. Mueller, *ibid.* **77**, 175 (1996).
[7] T.V. Ramakrishnan, Philos. Trans. R. Soc. London, Ser. A **356**, 41 (1998).
[8] D.M. Edwards, cond-mat/0201558 (unpublished); Adv. Phys. **51**, 1259 (2002).
[9] Y. Tokura and Y. Tomioka, J. Magn. Magn. Mater. **200**, 1 (1999).
[10] K. Kanamori, J. Appl. Phys. **31**, 14S (1960); J.B. Goodenough, Phys. Rev. **100**, 564 (1955).
[11] K. Kugel and D.I. Khomskii, JETP Lett. **15**, 446 (1972); Sov. Phys. JETP **37**, 725 (1973).
[12] H. Kuwahara, Y. Tomioka, A. Asamitsu, Y. Moritomo, and Y. Tokura, Science **270**, 961 (1995).
[13] H. Kuwahara, T. Okuda, Y. Tomioka, A. Asamitsu, and Y. Tokura, Phys. Rev. Lett. **82**, 4316 (1999).
[14] Y. Tomioka, A. Asamitsu, Y. Moritomo, H. Kuwahara, and Y. Tokura, Phys. Rev. Lett. **74**, 5108 (1995).
[15] J. Hejtmanek, E. Pollert, Z. Jirk, D. Sedmidubsk, A. Strejc, A. Maignan, Ch. Martin, V. Hardy, R. Kuzel, and Y. Tomioka, Phys. Rev. B **66**, 014426 (2002).
[16] Y. Tomioka, A. Asamitsu, H. Kuwahara, Y. Moritomo, and Y. Tokura, Phys. Rev. B **53**, R1689 (1996).
[17] A. Urushibara, Y. Moritomo, T. Arima, A. Asamitsu, G. Kido, and Y. Tokura, Phys. Rev. B **51**, 14 103 (1995).
[18] M. Imada, A. Fujimori, and Y. Tokura, Rev. Mod. Phys. **70**, 1039 (1998).
[19] Andrzej M. Oles, Mario Cuoco, and N.B. Perkins, in *Lectures on the Physics of Highly Correlated Electron Systems IV*, edited by F. Mancini, AIP Conf. Proc. No. 527 (AIP, Melville, NY, 2000).
[20] T. Akimoto, Y. Maruyama, Y. Moritomo, A. Nakamura, K. Hirota, K. Ohoyama, and M. Ohashi, Phys. Rev. B **57**, R5594 (1998).
[21] H. Kawano, R. Kajimoto, H. Yoshizawa, Y. Tomioka, H. Kuwahara, and Y. Tokura, Phys. Rev. Lett. **78**, 4253 (1997).
[22] R. Kajimoto, H. Yoshizawa, H. Kawano, H. Kuwahara, Y. Tokura, K. Ohoyama, and M. Ohash, Phys. Rev. B **60**, 9506 (1999).
[23] Z. Jirac, S. Krupika, V. Nekvasil, E. Pollert, G. Villeneuve, and F. Zounov, J. Magn. Magn. Mater. **15-18**, 519 (1980); Z. Jirak, S. Krupicka, Z. Simsa, M. Dlouha, and S. Vratislav, *ibid.* **53**, 153 (1985).
[24] J. Hejtmanek, Z. Jirak, E. Pollert, D. Sedmidubsky, A. Strec, C. Martin, A. Maignan, and V. Hardy, J. Appl. Phys. **91**, 8275 (2002).
[25] R. Kajimoto, H. Yoshizawa, Y. Tomioka, and Y. Tokura, cond-mat/0110170 (unpublished); Phys. Rev. B **66**, 180402(R) (2002).
[26] H. Yoshizawa, H. Kawano, J.A. Fernandez-Baca, H. Kuwahara, and Y. Tokura, Phys. Rev. B **58**, R571 (1998).
[27] M.V. Zimmermann, C.S. Nelson, J.P. Hill, Doon Gibbs, M. Blume, D. Casa, B. Keimer, Y. Murakami, C.-C. Kao, C. Venkataraman, T. Gog, Y. Tomioka, and Y. Tokura, Phys. Rev. B **64**, 195133 (2001).
[28] H. Kawano, R. Kajimoto, H. Yoshizawa, J.A. Fernandez-Baca, Y. Tomioka, H. Kuwahara, and Y. Tokura, Physica B **241-243**, 289 (1998).
[29] S. Ishihara, I. Inoue, and S. Maekawa, Physica C **263**, 130 (1996); Phys. Rev. B **55**, 8280 (1997).
[30] R. Maezono, S. Ishihara, and N. Nagaosa, Phys. Rev. B **57**, R13 993 (1998).
[31] R. Maezono, S. Ishihara, and N. Nagaosa, Phys. Rev. B **58**, 11 583 (1998).
[32] D. Khomskii and G.A. Sawatzky, Solid State Commun. **102**, 87 (1997).
[33] J. van den Brink, G. Khaliullin, and D. Khomskii, cond-mat/0206053 (unpublished); Phys. Rev. Lett. **83**, 5118 (1999).
[34] J.C. Slater and G.F. Koster, Phys. Rev. **94**, 1498 (1954).
[35] M.V. Zimmermann, J.P. Hill, Doon Gibbs, M. Blume, D. Casa, B. Keimer, Y. Murakami, Y. Tomioka, and Y. Tokura, Phys. Rev. Lett. **83**, 4872 (1999).
[36] M. Uehara, S. Mori, C.H. Chen, and S.-W. Cheong, Nature (London) **399**, 560 (1999); V. Podzorov, M. Uehara, M.E. Greshenson, T.Y. Koo, and S.-W. Cheong, Phys. Rev. B **61**, R3784 (2000).
[37] *Colossal Magnetoresistance, Charge Ordering and Related Properties of Manganese Oxides*, edited by C.N.R. Rao and B. Raveau (World Scientific, Singapore, 1998).
[38] J.C. Loudon, N.D. Mathur, and P.A. Midgley, Nature (London) **420**, 797 (2002).
[39] Z. Jirac, J. Hejtmanek, K. Knizek, M. Marysko, C. Martin, A. Maignan, and M. Hervieu, cond-mat/0212517 (unpublished).
[40] S. Misra, R. Pandit, and S. Satpathy, Phys. Rev. B **56**, 2316 (1997); J. Phys.: Condens. Matter **11**, 8561 (1999).
[41] A. Moreo, S. Yunoki, and E. Dagotto, Science **283**, 2034 (1999).
[42] E.L. Nagaev, *Physics of Magnetic Semiconductors* (Mir, Moscow, 1979); Sov. Phys. JETP **30**, 693 (1970); Physica B **230-232**, 816 (1997); Phys. Usp. **39**, 781 (1996).
[43] M. Yu Kagan, D.I. Khomskii, and M.V. Mostovoy, Eur. Phys. J. B **12**, 217 (1999); M. Yu Kagan, K.I. Kugel, and D.I. Khomskii, J. Exp. Theor. Phys. **93**, 415 (2001).
[44] D.P. Arovas and F. Guinea, Phys. Rev. B **58**, 9150 (1998); F. Guinea, G. Gomez-Santos, and D.P. Arovas, *ibid.* **62**, 391 (2000).
[45] J.L. Alonso, L.A. Ferdinandez, F. Guinea, V. Laliena, and V. Martin-Mayor, Phys. Rev. B **63**, 064416 (2000).
[46] S. Yunoki, J. Hu, A.L. Malvezzi, A. Moreo, N. Furukawa, and E. Dagotto, Phys. Rev. Lett. **80**, 845 (1998); S. Yunoki, A. Moreo, and E. Dagotto, *ibid.* **81**, 5612 (1998).
[47] E. Dagotto, J. Burgy, and A. Moreo, cond-mat/0209689 (unpublished) and references therein.
[48] Ch. Renner, G. Aeppli, B.-G. Kim, Y-Ah Soh, and S.-W. Cheong, Nature (London) **416**, 518 (2002).
[49] Y. Moritomo, Phys. Rev. B **60**, 10 374 (1999).
[50] Tulika Maitra and A. Taraphder, Europhys. Lett. **59**, 896 (2002).
[51] J. van den Brink and D. Khomskii, Phys. Rev. Lett. **82**, 1016 (1999).
[52] N. Furukawa, J. Phys. Soc. Jpn. **67**, 2734 (1995); also in Ref. 1 and references therein.
[53] K. Kubo and N. Ohata, J. Phys. Soc. Jpn. **33**, 21 (1972).
[54] In BK's convention for different spin ordering, $\theta_{xy} < \theta_z$ implies *A* phase. It is apparent, therefore, when both θ_{xy}, $\theta_z \simeq \pi$ but $\theta_{xy} < \theta_z$, a canted *A* phase, obtains. This is particularly important as the typical values of canting are quite large in BK. Conversely, from the structure of spin arrangements, such a state should be more appropriately called a canted *G* phase, although a *G* phase with such large canting has not been seen experimentally. This

ambiguity is easily resolved if in addition one considers orbital ordering.

[55] T. Hotta, A. Malvezzi, and E. Dagotto, Phys. Rev. B **62**, 9432 (2000).

[56] S. Satpathy, Zoran S. Popovic, and Filip R. Vukajlovic, Phys. Rev. Lett. **76**, 960 (1996).

[57] G. Venkateswara Pai, Phys. Rev. B **63**, 064431 (2001).

[58] L.F. Feiner and A.M. Oles, Phys. Rev. B **59**, 3295 (1999).

[59] R. Maezono *et al.* (Refs. 30 and 31), though, quote a lesser value of $J_{AF}=0.01t$, the reason for which is a possible use of AFM transition temperatures to ascertain it.

[60] The changes in $\theta_{xy,z}$ for small electron doping are small and depend weakly on y. Furthermore, the change in SE energy depends quadratically on the changes in $\theta_{xy,z}$.

[61] A. Maignan, C. Martin, F. Damay, and B. Raveau, Phys. Rev. B **58**, 2758 (1998); R. Mahendiran, A. Maignan, C. Martin, M. Hervieu, and B. Raveau, *ibid.* **62**, 11 644 (2000). It is not clear though if there is phase separation between different magnetic phases in these regions rather than canting.

[62] The complicated orbital order of this phase is beyond the homogeneous mean-field approach used. So this spin order can hardly be called the conventional CE phase. The $(\pi,\pi,0)$ CO associated with the CE phase was not obtainable from the long-range interaction used here either.

[63] R. Maezono, S. Ishihara, and N. Nagaosa, Phys. Rev. B **58**, 11 583 (1998).

[64] I.V. Solovyev and K. Terakura, Phys. Rev. B **63**, 174425 (2001).

[65] L. Sheng and C.S. Ting, cond-mat/9812374 (unpublished).

[66] H.Y. Hwang, P. Dai, S-W. Cheong, G. Aeppli, D.A. Tennant, and H.A. Mook, Phys. Rev. Lett. **80**, 1316 (1998).

[67] K.H. Ahn, X.W. Wu, K. Liu, and C.L. Chien, J. Appl. Phys. **81**, 5505 (1997).

[68] J. Blasco, J. Garca, J.M. de Teresa, M.R. Ibarra, J. Perez, P.A. Algarabel, C. Marquina, and C. Ritter, Phys. Rev. B **55**, 8905 (1997).

[69] J.L. Alonso, L.A. Fernandez, F. Guinea, V. Laliena, and V. Martin-Mayor, cond-mat/0111244 (unpublished).

[70] V. Cerovsky, S.D. Mahanti, T.A. Kaplan, and A. Taraphder, Phys. Rev. B **59**, 13 977 (1999).

[71] J. Dho, W.S. Kim, and N.H. Hur, Phys. Rev. Lett. **89**, 027202 (2002).

[72] Q. Yuan, T. Yamamoto, and P. Thalmeier, Phys. Rev. B **62**, 12 696 (2000).

[73] G. Jackeli, N.B. Perkins, and N.M. Plakida, Phys. Rev. B **62**, 372 (2001).

[74] T.V. Ramakrishnan, H.R. Krishnamurthy, M. Hassan, and G.V. Pai, in *Colossal Magnetoresistive Manganites*, edited by T. Chatterji (Kluwer Academic Publishers, Dordrecht, Netherlands, 2003); cond-mat/0308396 (unpublished) appear to justify quantitatively the ineffectiveness of JT physics for large x.

[75] Unjong Yu, Yookyung Jo, and B.I. Min, Physica B **328**, 117 (2003).

[76] C.D. Ling, J.E. Millburn, J.F. Mitchell, D.N. Argyriou, J. Linton, and H.N. Bordallo, Phys. Rev. B **62**, 15 096 (2000).

[77] Tulika Maitra and A. Taraphder, Europhys. Lett. (to be published); cond-mat/0308108 (unpublished).

[78] C. Castellani, C.R. Natoli, and J. Ranninger, Phys. Rev. B **18**, 4945 (1978); S. Inagaki, J. Phys. Soc. Jpn. **39**, 596 (1975); S.K. Ghatak and D.K. Ray, Phys. Rev. B **31**, 3064 (1985).

[79] Tulika Maitra and A. Taraphder (unpublished).

[80] The CE phase close to $x\leqslant 0.5$ appears in some cases in a narrow region for the intermediate-bandwidth systems (Refs. 20, 21, and 25). For $(La_{1-z}Nd_z)_{1-x}Sr_xMnO_3$, the region ($z\leqslant 0.54$ and $x\geqslant 0.5$) shows no charge ordering [see Fig. 1(b) in the present paper and Fig. 4 in Ref. 20].

[81] R. Maezono, S. Ishihara, and N. Nagaosa, Phys. Rev. B **57**, R13 993 (1998).

[82] In the choice of $J_H S_0$ in Eq. (3), there is an additional factor of 2 in Ref. 57.